The Astrophysical Journal, 922:110 (12pp), 2021 December 1 https://doi.org/10.3847/1538-4357/ac2610

Binary Black Hole Formation with Detailed Modeling: Stable Mass Transfer Leads to Lower Merger Rates

Monica Gallegos-Garcia[1,2], Christopher P L Berry[1,2,3], Pablo Marchant[4], and Vicky Kalogera[1,2]
[1] Department of Physics and Astronomy, Northwestern University, 2145 Sheridan Road, Evanston, IL 60208, USA
[2] Center for Interdisciplinary Exploration and Research in Astrophysics (CIERA),1800 Sherman, Evanston, IL 60201, USA
[3] SUPA, School of Physics and Astronomy, University of Glasgow, Glasgow G12 8QQ, UK
[4] Institute of Astrophysics, KU Leuven, Celestijnenlaan 200D, B-3001, Leuven, Belgium
Received 2021 July 12; revised 2021 September 10; accepted 2021 September 11; published 2021 November 24

Abstract

Rapid binary population synthesis codes are often used to investigate the evolution of compact-object binaries. They typically rely on analytical fits of single-star evolutionary tracks and parameterized models for interactive phases of evolution (e.g., mass transfer on a thermal timescale, determination of dynamical instability, and common envelope) that are crucial to predict the fate of binaries. These processes can be more carefully implemented in stellar structure and evolution codes such as MESA. To assess the impact of such improvements, we compare binary black hole mergers as predicted in models with the rapid binary population synthesis code COSMIC to models ran with MESA simulations through mass transfer and common-envelope treatment. We find that results significantly differ in terms of formation paths, the orbital periods and mass ratios of merging binary black holes, and consequently merger rates. While common-envelope evolution is the dominant formation channel in COSMIC, stable mass transfer dominates in our MESA models. Depending upon the black hole donor mass, and mass-transfer and common-envelope physics, at subsolar metallicity, COSMIC overproduces the number of binary black hole mergers by factors of 2–35 with a significant fraction of them having merger times orders of magnitude shorter than the binary black holes formed when using detailed MESA models. Therefore we find that some binary black hole merger rate predictions from rapid population syntheses of isolated binaries may be overestimated by factors of $\sim$ 5–500. We conclude that the interpretation of gravitational-wave observations requires the use of detailed treatment of these interactive binary phases.

Unified Astronomy Thesaurus concepts: Gravitational wave sources (677); Stellar mass black holes (1611); Stellar evolutionary models (2046); Roche lobe overflow (2155); Common envelope evolution (2154)

1. Introduction

Binary black hole (BBH) mergers have now been detected through gravitational-wave (GW) observations (Abbott et al. 2016). The LIGO Scientific and Virgo Collaboration (LVC) have completed the third observing run, and their current catalog contains over 50 GW candidates from compact-object coalescences, where 47 correspond to BBH mergers (Abbott et al. 2019, 2021a, 2021b). Several independent groups have analyzed the public GW data set (Abbott et al. 2021c) and found additional BBH candidates (Venumadhav et al. 2019; Zackay et al. 2019b, 2019a; Venumadhav et al. 2020; Nitz et al. 2020, 2021). In the coming years, the sample of BBH mergers will grow rapidly as the sensitivity of the GW detectors improves (Abbott et al. 2020). Once we have collected a sample of hundreds of detections, the challenge will be to accurately interpret and understand these observations.

An outstanding question is how the detected BBHs formed—many channels have been proposed. These can broadly be separated into two categories: isolated binary evolution and formation involving dynamical interactions. Isolated binary evolution includes formation following a common-envelope (CE) or stable mass-transfer (MT) phase (Paczynski 1976; van den Heuvel 1976; Tutukov & Yungelson 1993; Belczynski et al. 2002; Dominik et al. 2012; Stevenson et al. 2017; Giacobbo & Mapelli 2018; van den Heuvel et al. 2017; Neijssel et al. 2019; Vigna-Gómez et al. 2020; Bavera et al. 2021), or following chemically homogeneous evolution (de Mink & Mandel 2016; Mandel & de Mink 2016; Marchant et al. 2016; du Buisson et al. 2020; Riley et al. 2021), and may include Population III stars (Belczynski et al. 2004; Kinugawa et al. 2014; Inayoshi et al. 2017). Formation of merging BBHs through dynamical interactions includes systems within globular clusters (Kulkarni et al. 1993; Sigurdsson & Hernquist 1993; Portegies Zwart & McMillan 2000; Rodriguez et al. 2015, 2021; Fragione & Kocsis 2018; Di Carlo et al. 2019), isolated triple and quadruple systems (Thompson 2011; Antonini et al. 2017; Fragione & Kocsis 2019; Vigna-Gómez et al. 2021), young stellar clusters (Rastello et al. 2020; Banerjee 2021; Trani et al. 2021), nuclear star clusters (Antonini & Rasio 2016; Arca-Sedda & Gualandris 2018; Zhang et al. 2019), and within disks of active galactic nuclei (Stone et al. 2017; Bartos et al. 2017; Fragione et al. 2019; Gröbner et al. 2020; Kaaz et al. 2021). The overall population likely includes a mix of channels (Zevin et al. 2021), and understanding observations requires detailed modeling of each.

We focus on the isolated binary evolution of BBHs through CE evolution and stable MT (for a review, see Postnov & Yungelson 2014; Mapelli 2018). To interpret GW observations through any channel requires simulation of large binary populations, and hence the use of population synthesis codes. To model stellar and binary evolution efficiently, many population synthesis codes implement single-star evolution formulae based upon Hurley et al. (2000) combined with prescriptions to model binary evolution physics. These include BSE (Hurley et al. 2002), StarTrack (Belczynski et al. 2002, 2008), binary_c (Izzard et al. 2004, 2006, 2009), MOBSE (Giacobbo & Mapelli 2018; Giacobbo et al. 2018), COMPAS (Stevenson et al. 2017; Barrett et al. 2018), and the Compact Object Synthesis and Monte Carlo

Investigation Code (COSMIC; Breivik et al. 2020). Similarly, SEBA (Portegies Zwart & Verbunt 1996; Nelemans et al. 2001) uses the formulae based upon Eggleton et al. (1989). Others such as BPASS (Eldridge & Stanway 2009; Eldridge et al. 2017; Stanway & Eldridge 2018), SEVN (Spera et al. 2015, 2019), COMBINE (Kruckow et al. 2018), and METISSE (Agrawal et al. 2020) use a variety of more detailed stellar evolution models. Population synthesis codes such as these have been instrumental in advancing our understanding of double compact-object populations for the past few decades.

Although binary populations synthesis codes have been necessary to statistically study compact-object formation, they also have uncertainties and shortcomings. Some uncertainties, such as in stellar winds (Renzo et al. 2017; Vink & Sander 2021), reflect an incomplete understanding of the relevant physics involved (for a review of massive star winds, see Puls et al. 2008). However, other uncertainties, such as in MT stability and efficiency (García et al. 2021; Olejak et al. 2021) or the mass boundary at which CE evolution terminates (Han et al. 1994; Dewi & Tauris 2000; Ivanova 2011), may be improved by using detailed modeling of binary evolution. Understanding these sources of uncertainty is central to accurately interpreting observations.

Recently, detailed simulations of binary evolution have shown that MT is stable over wide ranges in orbital period and mass ratio, avoiding CE (Woods & Ivanova 2011; Ge et al. 2015; Pavlovskii et al. 2017; van den Heuvel et al. 2017; Marchant et al. 2021). Using the state-of-the-art stellar evolution code Modules for Experiments in Stellar Astrophysics (MESA; Paxton et al. 2011, 2013, 2015, 2019) some studies have concluded that the occurrence of successful CE leading to BBH merger may be overestimated in population synthesis codes (Klencki et al. 2020, 2021; Marchant et al. 2021). Klencki et al. (2021) showed that even with optimistic assumptions for CE, only donors with convective envelopes survive a CE phase. In addition, Klencki et al. (2020) showed that a specific stellar phase (e.g., core helium burning stars, Hertzsprung gap stars) does not directly correlate with a convective envelope, an assumption often made in population synthesis codes. Marchant et al. (2021) modeled MT and CE evolution of a massive 30 $M_{\odot}$ main-sequence (MS) donor with varying point-mass companions at a wide range of orbital periods. They found that stable MT dominates the formation rate of merging BBHs. Similar results are shown with population synthesis codes using updated CE stability criteria (Neijssel et al. 2019; Olejak et al. 2021; Shao & Li 2021). In an effort to include up-to-date methods of binary evolution into studies of large binary populations, groups have implemented hybrid methods in their studies. These methods typically use population synthesis codes combined with detailed simulations of stellar and binary evolution (Nelson 2012; Chen et al. 2014; Shao et al. 2019; Bavera et al. 2021; Román-Garza et al. 2021; Zapartas et al. 2021; Shao & Li 2021). These studies show that including more detailed modeling of binary interactions may reveal details that are missed using simpler prescriptions.

We use a hybrid approach to study the effect of detailed modeling of stellar and binary physics on BBH mergers. We address the question: how will the formation of merging BBHs be affected if we use detailed simulations instead of the prescriptions of COSMIC to model the evolution of hydrogen-rich donors with black hole companions (BH–H-rich star binaries)? Using similar binary evolution treatment as Marchant et al. (2021), we compare predicted BBH mergers between the rapid population synthesis code COSMIC and MESA models. With this comparison, we approximate how the rate of BBH mergers would be affected and identify qualitative differences in the resulting populations. In Section 2 we describe our comparison and the stellar and binary assumptions made. In Section 3 we describe our model variations, and in Section 4 we show the outcomes of our binary simulations ran with MESA. In Section 5 we provide a qualitative comparison between the outcomes found with MESA to the same binary systems simulated with COSMIC. In Section 6 we present our quantitative comparisons between binary populations ran with COSMIC to those informed by our detailed simulations. We find that the dominant formation channel is stable MT across the range of masses we consider, and that the merger times for BBH differ between COSMIC and our detailed simulations with MESA. Consequently, merger rates from isolated binary evolution calculated using current population synthesis prescriptions may be significantly overestimated.

2. Method

We compare BBH mergers between the rapid population synthesis code COSMIC, and detailed MESA binary evolutionary models. COSMIC is based on BSE, which uses stellar evolutionary models from Pols et al. (1998) and Hurley et al. (2000, 2002) and includes some updates to massive star evolution (Breivik et al. 2020; Zevin et al. 2020). MESA is a one-dimensional stellar evolution code that also includes physical prescriptions for binary stellar evolution (Paxton et al. 2011, 2013, 2015, 2019). In Section 2.1 we describe how we combine an initial population of binaries from the code COSMIC with detailed grids of MESA simulations to perform this comparison. In Sections 2.2 and 2.3 we describe our stellar and binary physics models and assumptions. Since our objective is to assess how detailed modeling of the BH–H-rich star stage affects the final evolutionary outcome, we are careful to maintain consistency in all other areas of stellar and binary physics between the two codes. Our simulations are computed using version 12115 of MESA, and version 3.3 of COSMIC.

2.1. Relative Rate Calculation

We use COSMIC to generate an initial population of binaries formed from a single burst of star formation with binary parameters initialized following Moe & Di Stefano (2017). We evolve these binaries from zero-age MS (ZAMS) until the formation of a hydrogen-rich donor with a BH companion (BH–H-rich star). To compare binary evolution for different donor masses, we create subpopulations by selecting systems where the H-rich donor is in a specified mass range, e.g., $M_{\rm donor} = (25 \pm 2.5)\ M_{\odot}$, and with a mass ratio $q = M_{\rm accretor}/M_{\rm donor}$, $q < 1$. We consider four subpopulations of BH–H-rich star binaries with different donor mass ranges: $M_{\rm donor} = (25 \pm 2.5)\ M_{\odot}$, $(30 \pm 2.5)\ M_{\odot}$, $(35 \pm 2.5)\ M_{\odot}$, and $(40 \pm 2.5)\ M_{\odot}$.

We compute the subsequent evolution of the BH–H-rich star binaries with both COSMIC and MESA. Using COSMIC, we continue the evolution of the binaries from our initial population. For MESA, instead of simulating each unique binary system within our COSMIC subpopulation, we generate a grid of BH–MS binaries with varying mass ratio and initial orbital period for each of our four subpopulations. This means that we select a *single* donor mass in MESA to compare to a selected mass range

of COSMIC systems (i.e., a mass range of $M_{\rm donor} = (30 \pm 2.5)$ $M_\odot$ in our COSMIC models is compared to a single grid of MESA simulations with $M_{\rm donor} = 30$ $M_\odot$). We also simplify all H-rich stars in COSMIC as MS stars in MESA.

Given the final evolutionary state of the binaries modeled with COSMIC and MESA, we can identify differences in the orbital period and mass ratio for BH–H-rich star binaries that evolve to form merging BBHs. Combining this information with the number of BH–H-rich star binaries formed in the initial COSMIC population, we can estimate the number of merging BBHs. Using these results, we calculate a number ratio $\mathcal{N}$ for each donor mass,

$$\mathcal{N}(\tau) = \frac{N_{\rm mrg}^{\rm COSMIC}(\tau)}{N_{\rm mrg}^{\rm MESA}(\tau)}, \quad (1)$$

where $N_{\rm mrg}^{\rm COSMIC}(\tau)$ is the number of BBHs that merge at time τ resulting from binary systems evolved with COSMIC, and $N_{\rm mrg}^{\rm MESA}(\tau)$ is the number of BBH mergers following the BH–MS evolution with MESA including its detailed treatment of MT. We will primarily consider the number of mergers within a Hubble time ($\tau_{\rm H} = 13.8$ Gyr) and the ratio $\mathcal{N}(<\tau_{\rm H})$.

While $N_{\rm mrg}^{\rm COSMIC}$ can be calculated by counting the number of BBH mergers in the COSMIC simulation, to calculate $N_{\rm mrg}^{\rm MESA}$, we must combine the initial BH–H-rich star subpopulations from COSMIC and our grid of MESA models. For each donor mass range, we:

1. Bin the subpopulation of COSMIC BH–H-rich star systems in mass ratio and orbital period to compare to our MESA models. The size of bins is set to match the highest resolution of our MESA grids so that each bin corresponds to one MESA simulation.
2. Identify all bins where the outcome of their corresponding MESA simulation results in a BBH that merges within a Hubble time.
3. Assume that all of the COSMIC BH–H-rich systems evolved within these bins will result in a BBH merger.
4. Sum the total number of binaries in those bins.

The final sum is $N_{\rm mrg}^{\rm MESA}(<\tau_{\rm H})$, the number of BBH mergers resulting from the initial COSMIC population, but except now BH–H-rich star MT and CE is treated using MESA (see Section 6 for an illustration of this procedure). We have verified that the resolution of our MESA grid does not significantly influence our results.

To illustrate the difference in merger times, we calculate an estimated merger rate from a subpopulation

$$\mathcal{R}_{\rm mgr} = \sum_{i=1}^{N_{\rm mrg}(<\tau_{\rm H})} \frac{1}{t_{{\rm mrg},i}} = N_{\rm mrg}(<\tau_{\rm H}) \left\langle \frac{1}{t_{\rm mrg}} \right\rangle, \quad (2)$$

where the sum is over all binaries that merge within a Hubble time, the weighting is by the inverse of the binary's merger time $t_{{\rm mrg},i}$, and $\langle 1/t_{\rm mrg} \rangle$ is the mean inverse merger time for the population. We use this to calculate a *relative rate*,

$$\mathcal{R}_{\rm rel} = \frac{\mathcal{R}_{\rm mrg}^{\rm COSMIC}}{\mathcal{R}_{\rm mrg}^{\rm MESA}}. \quad (3)$$

The relative rate $\mathcal{R}_{\rm rel}$ does not directly correspond to the expected ratio of astrophysical merger rates. Calculating these requires simulating an evolving population with varying star formation and metallicity across the history of the universe. This is beyond the scope of this study. However, if $\mathcal{R}_{\rm rel}$ is close to 1, we expect the astrophysical rates predicted using COSMIC and detailed simulations to be similar, and the differences in modeling to have negligible impact, whereas a value of $\mathcal{R}_{\rm rel}$ different from 1 indicates a discrepancy in predictions.

2.2. Stellar Physics

The stellar physics in our MESA simulations is similar to what is implemented in the MESA Isochrones and Stellar Tracks library (MIST; Choi et al. 2016). Our standard models are initialized at a metallicity of $Z = 0.1$ $Z_\odot$, defining $Z_\odot = 0.0142$ and $Y_\odot = 0.2703$ (Asplund et al. 2009). We specify the helium fraction as $Y = Y_{\rm Big\ Bang} + (Y_\odot - Y_{\rm Big\ Bang})Z/Z_\odot$, where $Y_{\rm Big\ Bang} = 0.249$ (Ade et al. 2016). Nuclear reaction rates are drawn from the JINA Reaclib database (Cyburt et al. 2010). We use the `basic.net` nuclear reactions networks for H and He burning; `co_burn.net` for C and O burning, and `approx21.net` for later phases. We use the standard equation of states in MESA of OPAL (Rogers & Nayfonov 2002), HELM (Timmes & Swesty 2000), PC (Potekhin & Chabrier 2010), and SCVH (Saumon et al. 1995). Radiative opacities are taken from Iglesias & Rogers (1996), which include the impact of enhanced CO-mixtures in the opacities, as well as the opacity calculations of Ferguson et al. (2005) for low temperatures. Models are computed until they reach core carbon depletion (central ^{12}C abundance $< 10^{-2}$); at this point, we assume that stars will undergo direct core collapse to a BH with mass equal to their baryonic mass.

Stars are assumed to be synchronized with the orbital period at the beginning of the MESA simulations. The implementation of rotation in MESA closely follows Heger et al. (2000, 2005). We include rotational mixing with an efficiency parameter of $f_{\rm c} = 1/30$ (Heger et al. 2000; Chaboyer & Zahn 1992). We include transport of angular momentum by magnetic fields due to the Spruit–Tayler dynamo (Spruit 2002).

For convective mixing, we adopt the mixing-length theory of Mihalas (1978) and Kurucz (1970) with a convection mixing-length parameter $\alpha_{\rm MLT} = 1.93$ based on results from the MIST project (A. Dotter et al. 2021, in preparation). Convective boundaries are determined with the Ledoux criterion. We do not include semi-convection mixing and instead use convective premixing (Paxton et al. 2019, Section 5.2). MESA treats thermohaline mixing with a diffusion coefficient motivated by Ulrich (1972) and Kippenhahn et al. (1980). We adopt a thermohaline mixing efficiency parameter of $\alpha_{\rm th} = 17.5$, which follows Charbonnel & Zahn (2007) with an aspect ratio of 1 for the instability fingers. Overshoot mixing is treated with the exponential decay formalism (Herwig 2000; Paxton et al. 2011). For the range of stellar masses studied here, we use $f_{\rm ov} = 0.0415$, which describes the extent of the overshoot mixing in this formalism. This value is motivated by Brott et al. (2011), who used the step overshoot formalism, and the work of Claret & Torres (2017) is used to translate the step to exponential decay overshoot. To prevent numerical issues caused by radiation-dominated envelopes, such as those in massive stars, we use the MLT++ treatment of convection (Paxton et al. 2013, Section 7.3). While this treatment helps prevent numerical issues, it reduces the radius expansion and can affect MT for massive donors (Klencki et al. 2020). The use of the MLT++ treatment is in contrast to Marchant et al. (2021), but (as discussed in Section 4) we find consistent

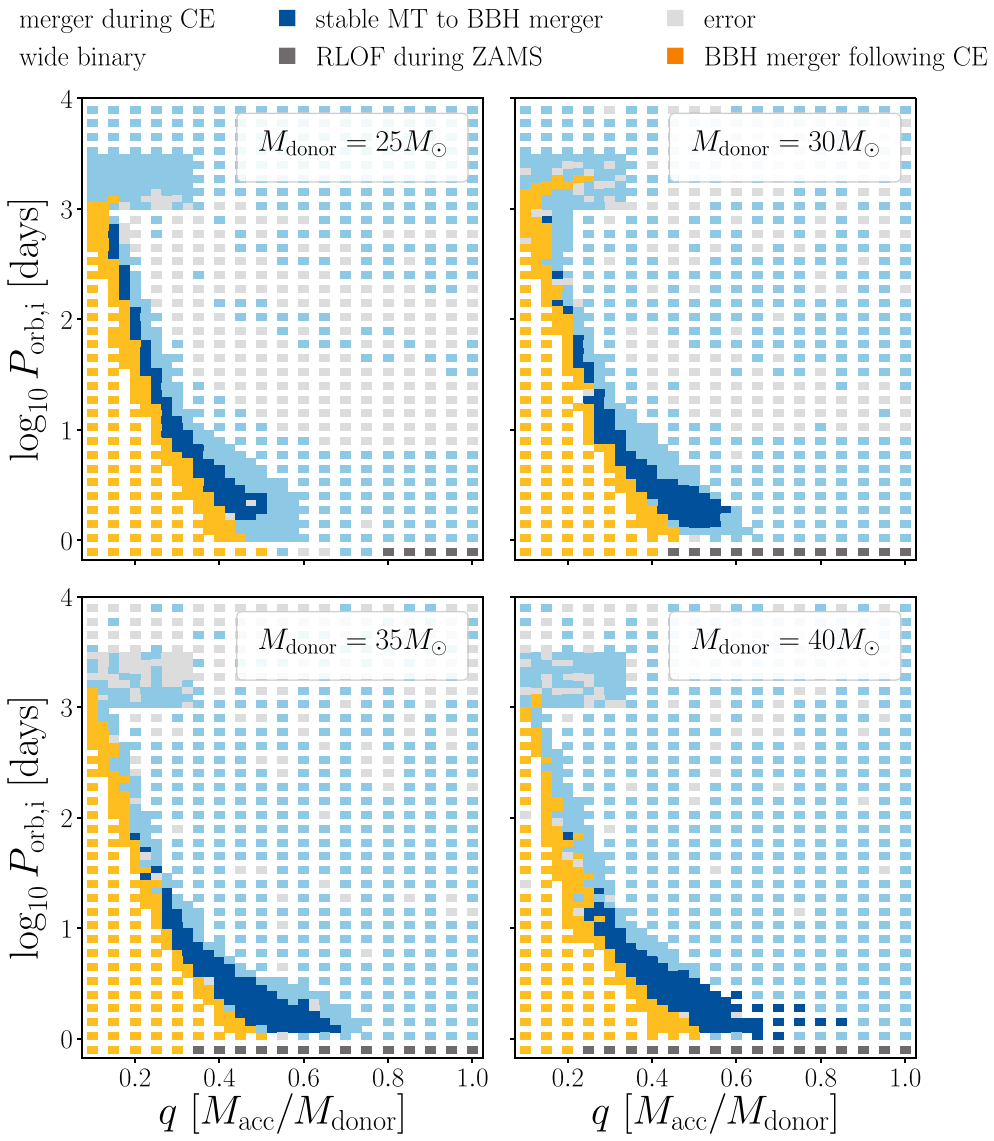

Figure 1. Final outcomes of our standard models of BH–MS systems ran with MESA. They have subsolar metallicity $Z = 0.1\ Z_\odot$, CE efficiency $\alpha_{\rm CE} = 1$, and no additional sources of energy into unbinding the envelope, $\alpha_{\rm th} = 0$. Each panel corresponds to a different donor mass. For all masses, we find a narrow band of systems whose outcome results in a BBH merger within a Hubble time following only a phase of stable MT (dark blue). For these models, we do not find any successful CE ejections.

results, indicating that our qualitative conclusions are not significantly impacted by this choice.

For stellar winds, we use the Dutch prescription in MESA, which is based on Glebbeek et al. (2009). It uses Vink et al. (2001) for effective temperatures of $T_{\rm eff} > 10^4$K and surface H mass fraction of $H > 0.4$; Nugis & Lamers (2000) for $T_{\rm eff} > 10^4$K and $H < 0.4$ (Wolf–Rayet stars), and de Jager et al. (1988) for $T_{\rm eff} < 10^4$K.

The COSMIC wind prescription most similar to the Dutch prescription treats O and B stars following Vink et al. (2001), and Wolf–Rayet stars following Hamann & Koesterke (1998) reduced by factor of 10 (Yoon et al. 2010) with metallicity scaling of $(Z/Z_\odot)^{0.86}$ (Vink & de Koter 2005). We expect the differences between the winds used for MESA and COSMIC to not significantly affect our results.

In COSMIC, instead of direct core collapse, we follow the delayed prescription of Fryer et al. (2012). Other models like the probabilistic prescription of Mandel & Müller (2020) or based upon the simulations of Patton & Sukhbold (2020) indicate that the delayed prescription of Fryer et al. (2012) may overestimate the amount of mass lost during the formation of the BH, resulting in lower-mass BHs (e.g., Patton et al. 2021). While this may have an impact on the GW inspiral times, it should not significantly affect the relative contribution of stable and unstable MT for BBH mergers. For both models ran with MESA and COSMIC, we do not introduce supernova (SN) kicks. However, our COSMIC models still have kicks from mass loss. The differences in SN prescriptions do not weaken our final results since the direct core-collapse method is on the more optimistic side of producing BBH mergers.

2.3. Binary Evolution Physics

In order to enable a more direct comparison between MESA and COSMIC, we make an effort to maintain consistency in all other parts of binary evolution modeling. However, notable differences in the computation of binary evolution between the two codes still exist. The primary differences stem from the ability of MESA to model binary evolution in more detail.

For both COSMIC and MESA, we initialize BH–MS binary systems with non-spinning BHs, but, unlike COSMIC, MESA evolves the spin-up of the BH through accretion (Marchant et al. 2017).

To compute the effect of tides in MESA, we apply a structure-dependent tidal torque summed throughout the whole star. Equilibrium tides are applied relative to convective zones (Hut 1981; Hurley et al. 2002) and dynamical tides connected to radiative zones. We use the tidal coefficient E_2 calculated in Qin et al. (2018), based upon Zahn (1977), to calculate the dynamical tides. Tides modeled in COSMIC follow Belczynski et al. (2008), which includes either equilibrium tides or dynamical tides based strictly upon the stellar type and mass (Hurley et al. 2002).

In both COSMIC and MESA, we assume conservative MT for sub-Eddington accretion onto a BH. In our standard model, we limit accretion to the Eddington limit and explore accretion limits up to 10 times the Eddington limit. We allow for Bondi–Hoyle accretion (Bondi & Hoyle 1944) and adopt an efficiency factor $\alpha_{\rm BH} = 1.5$, as in Hurley et al. (2002). Mass lost during super-Eddington MT is removed from the system with the specific angular momentum of the accretor.

BH–MS models ran with MESA remain in circular orbits during binary evolution while binary systems in COSMIC may be born with or gain eccentricity during kicks. However, our comparison begins at the BH–H-rich stage when the eccentricities of COSMIC systems are relatively low ($e \lesssim 0.2$). We have confirmed that the additional orbital angular momentum of these eccentric binaries, when translated to a corresponding circular orbit, did not significantly affect the results. For both codes, the evolution of orbital angular momentum considers the effects of mass loss, gravitational radiation (Peters & Mathews 1963), and tides as described above.

2.3.1. Common-envelope Evolution

A crucial difference between binary evolution modeled in COSMIC and MESA is how CE is initiated and treated. In COSMIC, CE evolution follows the classic $\alpha_{\rm CE}$–λ prescription (Webbink 1984; de Kool 1990; Dewi & Tauris 2000) with critical mass ratio $q_{\rm crit}$ values to determine the onset of CE. In MESA, we implement the detailed model for MT and CE evolution following the method of Marchant et al. (2021).

In our COSMIC simulations, we use the variable λ prescriptions by Claeys et al. (2014) set to include only gravitational potential energy to unbind the envelope $\lambda_{\rm g}$ (Dewi & Tauris 2000). Since the default behavior of the Claeys et al. (2014) λ prescription includes both gravitation and thermal energy, where it is approximated as $\lambda = 2\lambda_{\rm g}$, we scale the λ value by a factor of 1/2. Our standard COSMIC models are ran with $q_{\rm crit}$ following Belczynski et al. (2008). We also assume the optimistic CE scenario where systems with a Hertzsprung gap star can survive the CE phase (Belczynski et al. 2010). As a comparison, we also use the pessimistic scenario, where these same systems do not survive.

In the method of Marchant et al. (2021), the prescription for MT is an extension of the one developed by Ritter (1988) and Kolb & Ritter (1990), and accounts for cases of large overflow as well as potential outflows from outer Lagrangian points. To model the outcome of CE evolution, we follow a similar method to the usual $\alpha_{\rm CE}$–λ prescription, but aim to determine the binding energy self-consistently with the stellar model. Whenever a donor exceeds an MT rate of $\dot{M} > 1 M_\odot$ yr^{-1}, we consider MT to be unstable, and model the evolution as a CE system. At the onset of instability, we compute the binding energy outside an arbitrary mass coordinate m,

$$E_{\rm bind}(m) = \int_m^{M_{\rm donor}} \left(-\frac{Gm'}{r} + \alpha_{\rm th} u \right) dm', \tag{4}$$

where u is the specific internal energy of the gas, and $\alpha_{\rm th}$ represents the fraction of this energy that can be used for the ejection of the envelope. For consistency with the assumptions of our COSMIC models, we take $\alpha_{\rm th} = 0$. Given $E_{\rm bind}$ and the efficiency $\alpha_{\rm CE}$, one can determine the post-CE orbital separation if one knows the mass coordinate $M_{\rm core}$ at which the CE process completes; to determine this, we simulate a rapid mass-loss phase from the star while updating the separation of the binary using the binding energy at each mass coordinate, until the system detaches (Marchant et al. 2021, Section 2.2 therein).

3. Model Variations

The configurations in our standard COSMIC and MESA models are for metallicity $Z = 0.1\ Z_\odot$ and an effective CE efficiency of $\alpha_{\rm CE} = 1$. Parameters specific to COSMIC in our standard model include λ prescriptions by Claeys et al. (2014) and $q_{\rm crit}$ following Belczynski et al. (2008).

In addition to the standard model, we consider five additional models:

1. Z—We simulate systems at solar metallicity.
2. *accretion*—Simulations have shown that mass accretion onto a BH can exceed the Eddington limit (Begelman 2002; McKinney et al. 2014). Super-Eddington accretion has also been studied in the context of massive BH binaries in the pair-instability mass gap (van Son et al. 2020). We thus allow for super-Eddington accretion at 10 times the Eddington limit.
3. $\alpha_{\rm CE}$— We apply a higher CE efficiency of $\alpha_{\rm CE} = 5$. Three-dimensional hydrodynamical studies of successful envelope ejections have suggested $\alpha_{\rm CE}$ values as low as 0.1–0.5 for extended red supergiant progenitors (Law-Smith et al. 2020). However, some one-dimensional simulations of CE evolution that include additional energy sources like ionization and thermal energy suggest a high CE efficiency of 5 (Fragos et al. 2019). In addition to this, many studies have previously concluded that $\alpha_{\rm CE}$ values up to 5 are at least marginally preferred in order to match the GW observations (Giacobbo & Mapelli 2018; Santoliquido et al. 2021; Zevin et al. 2021). We therefore consider this higher CE efficiency in order to explore the more optimistic CE assumption.
4. $q_{\rm crit}$—Based on the system's mass ratio at the onset of Roche lobe overflow (RLOF), the stability criteria, $q_{\rm crit}$, determines if a system will undergo a CE event or if it will proceed with stable MT. In our variation, we use the $q_{\rm crit}$ prescription from Claeys et al. (2014), which allows more systems with a Hertzsprung gap donor to proceed with stable MT instead of CE. Instead of $q_{\rm crit} = 0.33$ for all H-rich donors, as in our standard configuration, Claeys et al. (2014) uses $q_{\rm crit} = 1$ for MS stars, $q_{\rm crit} = 0.21$ for Hertzsprung gap stars, $q_{\rm crit} = 0.33$ for core helium burning donors, and $q_{\rm crit} = 0.87$ for first giant branch stars, early asymptotic giant branch (AGB), and thermally pulsing

AGB. Changing the $q_{\rm crit}$ prescription also introduces a change to the MT rates (Breivik et al. 2020). This variation also uses MT rates consistent with Claeys et al. (2014), which implements higher MT rates during thermal-timescale MT.

5. *CE*—We apply the Pessimistic scenario that causes a subset of stellar types to merge during the CE phase (Belczynski et al. 2007). In COSMIC, these stellar types include MS, Hertzsprung gap, naked helium MS, naked helium Hertzsprung gap, and white dwarfs. However, recent work shows that the survivability of CE is more attributed to the type of envelope of the donor rather than the evolutionary type of the donor (Klencki et al. 2021; Marchant et al. 2021), and the type of envelope cannot be linked to specific stellar types (Klencki et al. 2020). Therefore, the Pessimistic model for CE used here is likely not restrictive enough.

The first three variations require generating new grids of MESA models along with new COSMIC populations, while the final two are specific to COSMIC (and other population synthesis codes). We compare these variations in COSMIC to our standard MESA model.

4. MESA Results

4.1. Standard Model

We computed four grids of models, one for each donor mass 25 $M_\odot$, 30 $M_\odot$, 35 $M_\odot$, and 40 $M_\odot$, consisting of an MS donor with a BH accretor in a circular orbit. The grids span a period range between $-0.1 < \log_{10}(P_{\rm orb,i}/{\rm days}) < 4$, and initial mass ratios $q = M_{\rm accretor}/M_{\rm donor}$ between 0.1 and 1. Figure 1 shows the final outcomes of our standard model of MESA simulations as a function of initial mass ratio q and initial orbital period. Each panel in Figure 1 corresponds to a different donor mass. At these masses, the outcomes show a consistent picture. The (yellow) region corresponding to merger during CE occupies the bottom left of these plots. The region where systems undergo CE evolution is roughly the same for all donor masses: it extends from low-period orbits with $q \simeq 0.5$ diagonally upward to $P_{\rm orb,i} \simeq 1000$ days and $q \simeq 0.15$. In addition to this region, we also find a hook of CE evolution for $M_{\rm donor} = 30\ M_\odot$ at $P_{\rm orb,i} \simeq 1000$ days. For all donor masses with our standard model, we do not find any successful CE ejections, and hence there are no BBHs formed from CE evolution. However, we do find a (dark blue) region where the final outcome is a BBH merger within a Hubble time following a phase of stable MT. This region forms a narrow transition between systems merging during CE and systems that end up as wide, non-merging BBHs (light blue). We do not distinguish wide binaries with stable MT from wide binaries with no interaction. As donor mass increases, the region corresponding to BBH merger following only stable MT shifts to lower initial orbital periods and extends to larger initial mass ratios. In all cases, we find that the only formation channel for BBH mergers is stable MT. In Section 5 we compare the grids ran with $M_{\rm donor} = 25\ M_\odot$ and 40 $M_\odot$ to grids produced with COSMIC.

The grid of systems with $M_{\rm donor} = 30\ M_\odot$ can be compared to the results in Marchant et al. (2021). Both show a hook of CE evolution at $P_{\rm orb,i} \approx 1000$ days. This hook of CE evolution in our grid is smaller, and unlike Marchant et al. (2021), this region of CE evolution does not result in any successful ejections. A key difference that affects the survivability of CE between Marchant et al. (2021) and this work is our exclusion of the thermal energy and recombination component in CE ejection. However, when including thermal and recombination energy, Marchant et al. (2021) did not find a significant number of successful CE ejections leading to merging BBH. They find that under the assumption of a flat distribution in mass ratio and a flat distribution in $\log_{10}P_{\rm orb,i}$ for their grid with $M_{\rm donor} = 30\ M_\odot$, the ratio of the number of CE simulations that produce merging BBHs to the number of stable MT simulations that produce merging BBHs is 0.017. Similar outcomes have also been shown under more extreme scenarios. Klencki et al. (2021) found that even under a set of optimistic assumptions about CE evolution, a successful CE ejection is only possible when the donor has a massive convective envelope.

Another feature in our results that can be directly compared to Marchant et al. (2021) is the (dark blue) region corresponding to BBH mergers following stable MT. Both this work and Marchant et al. (2021) show that the dominant formation channel for BBH mergers is through stable MT, and that this region becomes more narrow with increasing initial orbital period. Additionally, Marchant et al. (2021) found that the boundary between stable and unstable MT was robust under different thresholds of unstable MT. These results are in agreement with previous studies. Ge et al. (2015) also found a similar trend for the boundary between stable and unstable MT: the boundary allows for more stability with increasing stellar age (increasing initial orbital period in our grids). Using stability criteria based on the work of Ge et al. (2015) for MS and Hertzsprung gap stars, Neijssel et al. (2019) found that 80% of the BBH mergers are formed from stable MT, not CE. Similarly, Olejak et al. (2021) used criteria for the onset of CE derived from the simulations of Pavlovskii et al. (2017) to find that BBH formation could be dominated by stable MT without a CE, although this conclusion also depended upon the MT timescale. Shao & Li (2021) combined their BSE population synthesis with MT stability criteria derived from grids of simulations ran with MESA. They assume that a CE is initiated if the MT rate exceeds a critical value based upon either (i) the Eddington rate at the photon-trapping radius (Begelman 1979; King & Begelman 1999; Belczynski et al. 2008), or (ii) 2% of the donor mass per orbit of the donor overflows the second Lagrange point (Pavlovskii & Ivanova 2015; Ge et al. 2020), and find that ∼30%–70% of merging BBHs form from stable MT. These results highlight that CE evolution is not needed to form merging BBHs.

These models at $Z = 0.1\ Z_\odot$ with $M_{\rm donor} = 30$, 35, and 40 $M_\odot$ experience numerical issues after the depletion of core hydrogen. The numerical issues cause the star's radius to vary and core mass to increase but the donor regains stability and continues its post-MS evolution. The discontinuities seen in the (dark blue) region corresponding to BBH mergers following stable MT may be attributed to these numerical issues. However, we do not expect such issues to have significant affects on our main conclusions or the qualitative behavior across parameter space. Additionally, about 30% of the errors in the grid with $M_{\rm donor} = 25\ M_\odot$ occurred close to core carbon depletion. Since these occur outside our regions of interest, and do not influence our results, we did not resolve the errors to continue the evolution to carbon depletion.

4.2. Variations to Standard Model

As described in Section 3, we generated three more sets of grids where we varied the CE efficiency $\alpha_{\rm CE}$, allowed for super-Eddington MT, and changed to solar metallicity.

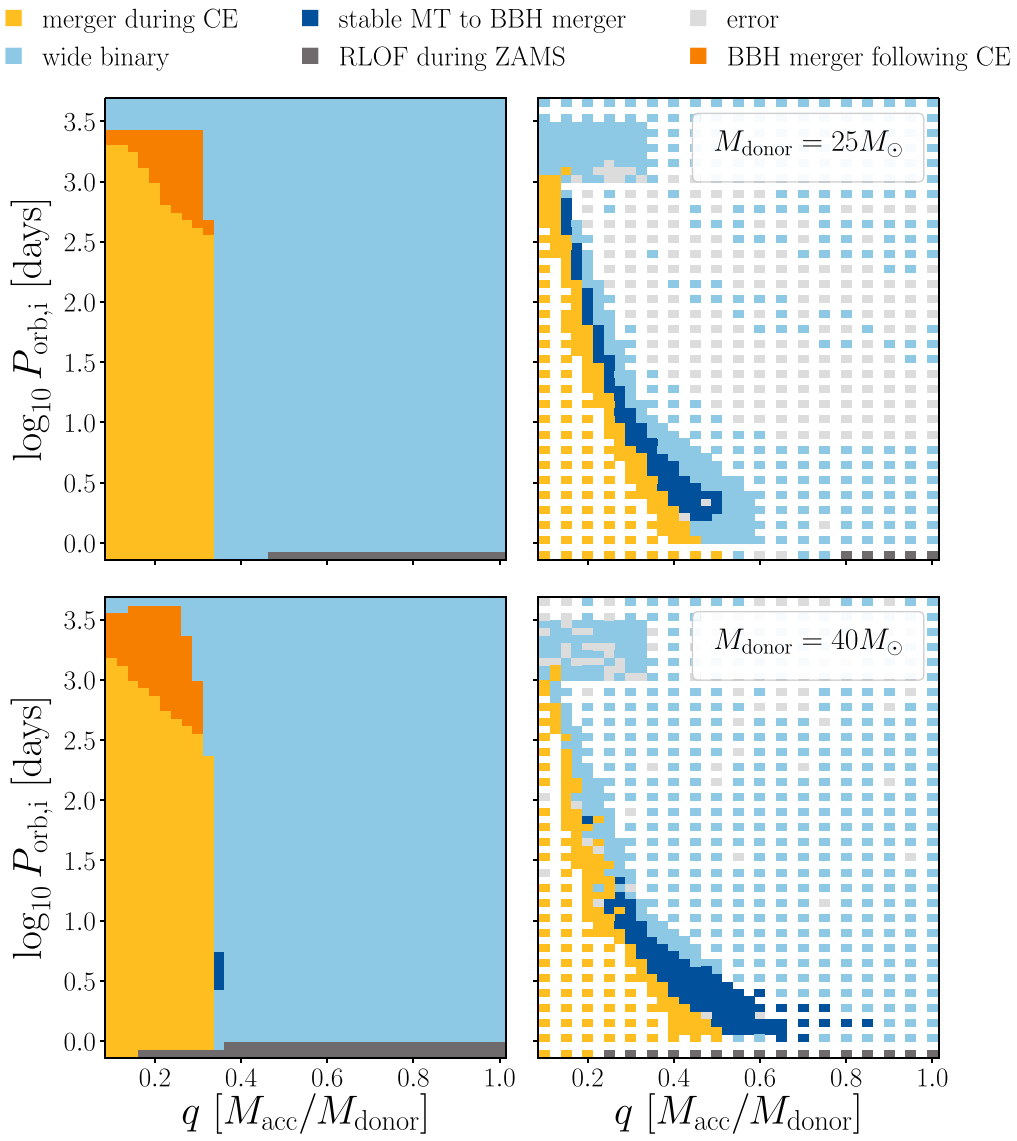

Figure 2. Comparison of final outcomes between binary simulations ran with COSMIC (left) to simulations ran with MESA (right). Top: comparison for MS–BH binaries with $M_{\rm donor} = 25\ M_\odot$ shown as a function of initial orbital period and mass rations, q. Bottom: same as top but for $M_{\rm donor} = 40\ M_\odot$. For binary evolution modeled with COSMIC, CE is the dominant formation channel for BBH mergers. For evolution modeled with MESA, we do not find any successful CE ejections, and all BBH mergers are formed through stable MT.

Increasing the CE efficiency from $\alpha_{\rm CE} = 1$ to $\alpha_{\rm CE} = 5$ (maintaining $\alpha_{\rm th} = 0$) results in little difference overall. However, for the grid with $M_{\rm donor} = 25\ M_\odot$, we find three simulations that result in a BBH merger following a successful CE ejection. These binaries are on the boundary between systems merging during the CE phase (yellow region) and simulations resulting in a BBH merger following stable MT (dark blue region). For $M_{\rm donor} = 30\ M_\odot$, we find successful CE ejections in the hook of CE evolution at $P_{\rm orb,i} \approx 1000$ days. For $M_{\rm donor} = 35\ M_\odot$, we do not find a difference when using $\alpha_{\rm CE} = 5$. For the grid of simulations with $M_{\rm donor} = 40\ M_\odot$, we find one system resulting in a BBH merger following CE.

Allowing for accretion at 10 times the Eddington limit, the regions where systems undergo a CE phase are similar to our standard models. We find more BBH mergers following stable MT at low initial orbital periods, roughly centered at low initial orbital periods $P_{\rm orb,i} \simeq 100$ days.

We find the greatest differences for the MESA models initialized at solar metallicity $Z = 0.0142$. Overall, we find fewer BBH mergers following stable MT and find fewer binaries undergoing CE. This is likely for two main reasons. First, strong stellar winds for solar metallicity widen the orbits compared to $Z = 0.1\ Z_\odot$. Therefore, fewer systems merge within a Hubble time, and we only find CE evolution for tighter initial orbital periods. Second, the radii of these stars are larger, causing RLOF during ZAMS at higher orbital periods. The only exception to an overall decrease in CE systems is for $M_{\rm donor} = 25$ and $40\ M_\odot$. In both of these cases, we find a hook of CE evolution at $P \sim 1000$ days, similar to the feature in Figure 1.

5. COSMIC and MESA comparison

Before combining MESA and COSMIC together to calculate the relative rates, we first compare BH–MS evolution from MESA to that with COSMIC. Although our relative rate calculation involves all BH–H-rich star binaries in COSMIC, including BH–MS, the differences presented here propagate

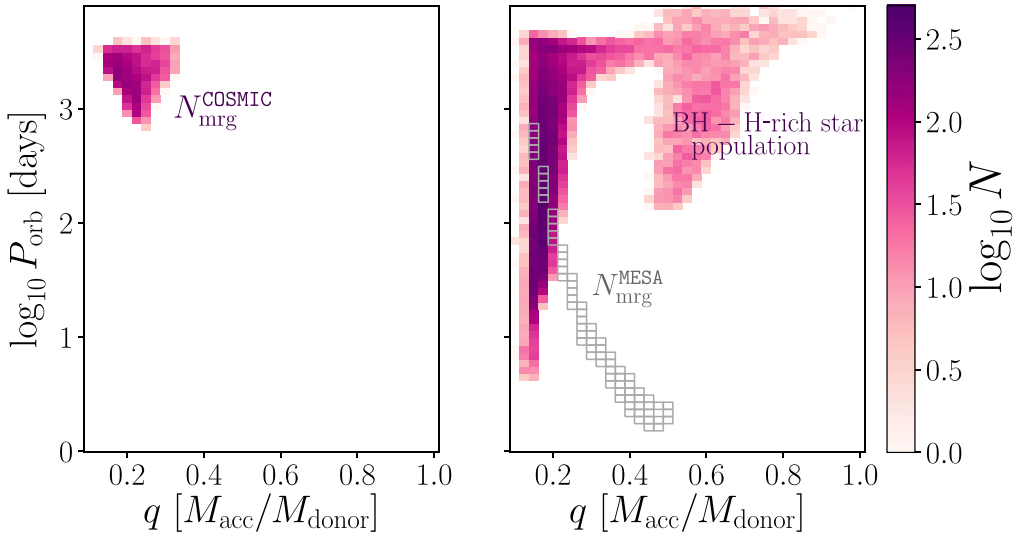

Figure 3. Method illustration for donor mass $M_{\mathrm{donor}} = (25 \pm 2.5)\ M_{\odot}$. Left: two-dimensional histogram of the final BBH merger population predicted by COSMIC as a function of mass ratio and orbital period when the system became a BH–H-rich star. The total number of binaries in this histogram is $N^{\mathrm{COSMIC}}_{\mathrm{mrg}}(<\tau_{\mathrm{H}})$. Right: two-dimensional histogram of BH–H-rich star population. Bins outlined in gray are regions where models ran with MESA result in BBH mergers. The sum of the number of BH–H-rich star binaries in these gray bins is $N^{\mathrm{MESA}}_{\mathrm{mrg}}(<\tau_{\mathrm{H}})$.

into the relative rate calculation, as they determine the regions of parameter space where merging BBHs can form.

Figure 2 shows the final outcomes of simulations for BH–MS binaries using our standard model. There are several key differences between our MESA and COSMIC simulations. First, we focus on outcomes involving CE evolution. We find that models ran with COSMIC develop strong interactions (e.g., CE interactions) at higher orbital periods ($P_{\mathrm{orb,i}} \sim 3000$ days) than models ran with MESA ($P_{\mathrm{orb,i}} \sim 1000$ days). The most frequent outcome are systems that result in a merger during the CE phase. In COSMIC, this (yellow) region extends from high initial orbital periods $P_{\mathrm{orb,i}} \sim 1000$ days at our lowest q to $P_{\mathrm{orb,i}} \sim 300$ days where it sharply cuts off at $q \sim 0.3$. This sharp boundary is a result of the q_{crit} prescription used in COSMIC to determine stable and unstable MT (Belczynski et al. 2008). For models ran with MESA, the same boundary between systems merging during CE and stable MT expands up to similar orbital periods as COSMIC, but instead of a sharp cutoff, the boundary sweeps from low q at high orbital periods gradually to $q \simeq 0.5$ at low orbital periods. MT stability increases with initial orbital period. In COSMIC we also find systems resulting in a BBH merger following a successful CE ejection. This (orange) region is isolated at $q \lesssim 0.3$ between $P_{\mathrm{orb,i}} \approx 300$–$3000$ days. With our standard MESA model, we do not find any simulations that result in a BBH merger following CE. Moreover, the region where COSMIC binaries result in BBH mergers following CE is predicted to be stable MT for binaries modeled with MESA. Thus, not only are BBH mergers following a successful CE ejection missing in MESA, most of this region does not develop unstable MT.

A second channel for BBH mergers is through stable MT (dark blue region). For the standard COSMIC models, this formation channel only occurs in the bottom panel with $M_{\mathrm{donor}} = 40\ M_{\odot}$. It is a small set of systems at $q \sim 0.35$ and $P_{\mathrm{orb,i}} \sim 5$ days. In contrast, this outcome occurs for a significant number of systems in the MESA grids. Most of these mergers occur at the boundary between stable and unstable MT, in a band that spans between $q \sim 0.2$–0.9, and widens with smaller initial orbital period.

Differences in the systems undergoing MT are expected because of (i) differences in stellar radius between the different stellar models (Agrawal et al. 2020), and (ii) differences in how MT impacts stellar structure. The difference in radii influences which stars undergo MT when. The differences in stellar structure arise because COSMIC effectively models the donor as a single star, with mass loss changing the mass and age of this single star (Hurley et al. 2000, Section 7.1). However, with detailed modeling, the structure of a star that has undergone MT is distinct from a single star of a comparable mass (e.g., Laplace et al. 2021). The addition of BBHs forming through stable MT mitigates some of the loss from CE evolution when comparing the total number of merging BBHs from our COSMIC population and the population simulated using MESA.

6. Relative Rate Calculation

Figure 3 illustrates how $N^{\mathrm{COSMIC}}_{\mathrm{mrg}}(<\tau_{\mathrm{H}})$ and $N^{\mathrm{MESA}}_{\mathrm{mrg}}(<\tau_{\mathrm{H}})$ are calculated. The left panel in Figure 3 shows a two-dimensional histogram of binaries from the BH–H-rich star subpopulation with $M_{\mathrm{donor}} = (25 \pm 2.5)\ M_{\odot}$ that results in BBH mergers within a Hubble time in COSMIC. We bin the population as a function of q and P_{orb} at the time the BH–H-rich binary was formed. The total number of binaries in the left panel is $N^{\mathrm{COSMIC}}_{\mathrm{mrg}}(<\tau_{\mathrm{H}})$. The right panel shows a two-dimensional histogram of the same BH–H-rich star subpopulation in COSMIC with $M_{\mathrm{donor}} = (25 \pm 2.5)\ M_{\odot}$. On this same histogram, we outline the bins in gray where BH–MS models ran with MESA result in a BBH merger within a Hubble time. The total number of BH–H-rich stars in COSMIC within these bins is $N^{\mathrm{MESA}}_{\mathrm{mrg}}(<\tau_{\mathrm{H}})$. The empty outlined bins do not contribute to the total. Table 1 shows our results for the number ratio $\mathcal{N}(<\tau_{\mathrm{H}}) = N^{\mathrm{COSMIC}}_{\mathrm{mrg}}(<\tau_{\mathrm{H}})/N^{\mathrm{MESA}}_{\mathrm{mrg}}(<\tau_{\mathrm{H}})$ for four different donor masses and six different models.

The first row in Table 1 shows the number ratio for our standard model. We find that $\mathcal{N}(<\tau_{\mathrm{H}})$ is between ∼1–8 across all donor masses (COSMIC produces up to eight times more merging BBHs). Another important difference is the dominant formation channel. The formation of BBH mergers for our

Table 1
Upper Limits of the Number Ratio $\mathcal{N}(<\tau_H) = N_{mrg}^{COSMIC}(<\tau_H)/N_{mrg}^{MESA}(<\tau_H)$ for All Model Variations and Donor Masses

	Subpopulation			
Model	25 $M_\odot$	30 $M_\odot$	35 $M_\odot$	40 $M_\odot$
Standard	1.3	4.3	7.8	2
$\dot{M}_{Edd} \times 10$	1.7	4	9	1.7
$\alpha_{CE} = 5$	2.6	15	35	8.5
$Z_\odot$	···	···	<0.06	0.4
Claeys	0.7	2.7	8.5	15
Pessimistic	1.3	4.3	7.7	2

Note. The last two rows correspond to variations that are specific to COSMIC. We compare these variations in COSMIC to the standard models ran with MESA. From top to bottom, the rows correspond to (1) standard model, (2) model allowing for an accretion rate onto the BH at 10× the Eddington limit, (3) CE efficiency $\alpha_{CE} = 5$ while keeping $\alpha_{th} = 0$, (4) solar metallicity, (5) q_{crit} criteria following Claeys et al. (2014), and (6) using the Pessimistic assumption for CE evolution.

standard COSMIC models form primarily through CE (∼ 99%) whereas our MESA models are solely by stable MT at these donor masses (see Figure 2).

The second row in Table 1 corresponds to the model allowing super-Eddington accretion at 10 times the Eddington limit. We find that higher accretion rates likely only affect low-period binaries with high accretion rates. In addition, Figure 3 shows that these low-period binaries do not affect our number ratio calculation since they occupy empty period–mass ratio bins. As a result, the number ratio with super-Eddington accretion is similar to the standard model.

The third row in Table 1 corresponds to the model with $\alpha_{CE} = 5$, while maintaining $\alpha_{th} = 0$. Compared to the standard model and the super-Eddington model, this model with higher CE efficiency results in more varied and higher values of the number ratio. For models ran with COSMIC, the value of α_{CE} used here was efficient enough to increase the number of BBH mergers without leading to wider binaries. On the other hand, for models ran with MESA at this higher α_{CE}, the formation of BBH mergers did not change significantly and is still significantly dominated by stable MT.

The fourth row in Table 1 corresponds to the number ratio for models ran at solar metallicity $Z = Z_\odot$. For H-rich donors at $M_{donor} = 25$ and 30 $M_\odot$, COSMIC did not produce any merging BBHs. For the grids of models with $M_{donor} = 25$ and 30 $M_\odot$ at solar metallicity, all of the BBH mergers found with MESA are outside of the initial COSMIC BH–H-rich star population (unlike the example shown in Figure 3). Therefore, for these donor masses, we cannot calculate $\mathcal{N}$. At $M_{donor} = 35$ $M_\odot$ and $M_{donor} = 40$ $M_\odot$, we find more merging BBHs with models ran with MESA than COSMIC. For $M_{donor} = 35$ $M_\odot$, we can calculate an upper limit (given the finite number of binaries in our population) of $\mathcal{N}(<\tau_H) < 0.06$, and for $M_{donor} = 40$ $M_\odot$ $\mathcal{N}(<\tau_H) = 0.4$.

The last two rows in Table 1 correspond to models where we vary parameters specific to COSMIC, and calculate a number ratio with the standard MESA model. In the fifth row, we change the q_{crit} prescription for MT stability from our standard model using Belczynski et al. (2008) to the prescription of Claeys et al. (2014). In this case, the number ratio varies from 0.7 for $M_{donor} = 25$ $M_\odot$ to 15 for $M_{donor} = 40$ $M_\odot$. Compared to the standard models, these subpopulations have significantly more BBHs mergers forming from BH–H-rich star systems with lower orbital periods between $P_{orb} \approx 10$–100 days and $q < 0.3$. Using the Claeys et al. (2014) prescription with

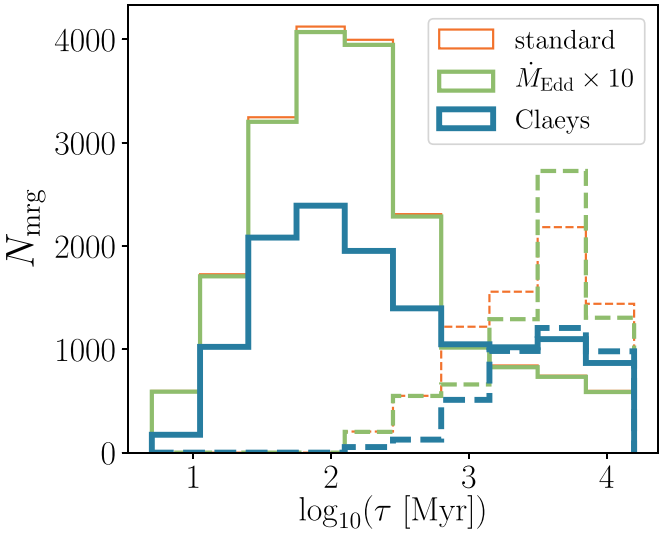

Figure 4. Histograms of N_{mrg} as a function of merger time τ for models ran with COSMIC (solid lines) and models using detailed stellar and binary simulations of BH–MS systems (dashed lines). We show the standard model in orange (thin line), the model allowing for an accretion rate onto the BH of $10 \times \dot{M}_{Edd}$ in green (medium line), and the model using q_{crit} criteria following Claeys et al. (2014) in COSMIC in blue (thick line). Here N_{mrg} includes all subpopulations per model. All models, except models with solar metallicity and $\alpha_{CE} = 5$, follow the same trend.

COSMIC, ∼ 77% of BBH mergers form through CE evolution and the rest through stable MT.

In the final row, we vary the survivability of CE by now assuming the Pessimistic CE scenario. This variation had no significant effect on the resulting number ratio for our COSMIC BBH merger populations at 0.1 $Z_\odot$. This is because the majority of binaries affected by this variation involve massive donors that expand significantly during the Hertzsprung gap (see also Dominik et al. 2012, Section 4.1). For our standard model in COSMIC, we find that these affected donors tend to be more massive than those considered in our calculation.

The changes in modeling between MESA simulations and COSMIC not only influence the number of merging binaries, but also when they merge. Figure 4 illustrates how N_{mrg}^{COSMIC} (solid lines) and N_{mrg}^{MESA} (dashed lines) vary for different merger times for three representative models. In Figure 4 we include all mass subpopulations per model as a proxy of the overall distribution across the mass range. In all cases (except models with solar metallicity and $\alpha_{CE} = 5$), we find that N_{mrg}^{COSMIC} is dominated by shorter merger times while N_{mrg}^{MESA} is dominated by longer merger times. These differences are due to the different dominate merger channels in each population. CE typically hardens the binary more efficiently than stable MT (Bavera et al. 2021), which leads to shorter merger times, peaking at $\lesssim$ 100Myr (Dominik et al. 2012; Eldridge & Stanway 2016), for BBH mergers formed through CE. We see a difference in the trend in the $\alpha_{CE} = 5$ model because the post-CE separation in the COSMIC systems is wider for $\alpha_{CE} = 5$ than in our standard model. There are also a few cases of successful CE evolution among the MESA results. In solar metallicity models, the enhanced mass loss from stellar winds results in lower-mass BH, which leads to longer merger times and a flatter distribution. The difference in merger times between CE evolution and stable MT will have an impact on the BBH merger rate across the history of the universe.

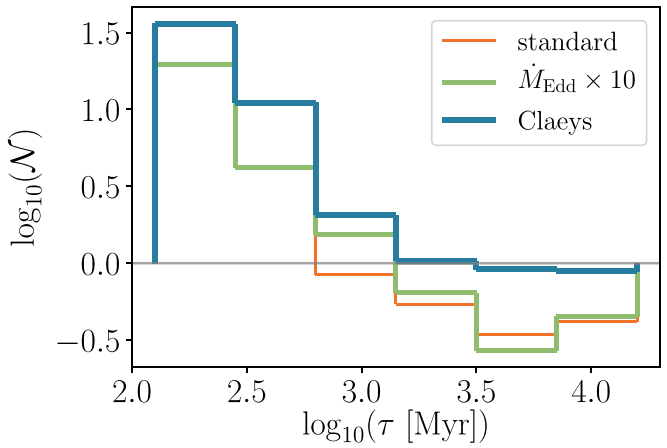

Figure 5. Same as Figure 4 but here we show the *number ratio* $\mathcal{N}$, the ratio of $N_{\rm mrg}^{\rm COSMIC}$ to $N_{\rm mrg}^{\rm MESA}$, binned as a function of merger time τ.

Table 2
Same as Table 1 but for $\mathcal{R}_{\rm rel}$, the Ratio of Our Estimated Subpopulation Merger Rate Calculated for COSMIC to the Estimated Merger Rate Calculated for MESA

	Subpopulation			
Model	25 $M_\odot$	30 $M_\odot$	35 $M_\odot$	40 $M_\odot$
Standard	6	187	400	145
$\dot{M}_{\rm Edd} \times 10$	7.1	128	607	142
$\alpha_{\rm CE} = 5$	0.24	168	554	293
$Z_\odot$	…	…	…	1.6
Claeys	5.7	80	422	744
Pessimistic	6	186	387	145

Note. Since the total number of mergers is typically not more than an order of magnitude greater with COSMIC than with MESA, a value $\gg 1$ corresponds to populations where COSMIC is much more dominated by shorter merger times.

To further compare the differences in merger times, in Figure 5 we show the values of number ratio $\mathcal{N} = N_{\rm mrg}^{\rm COSMIC}/N_{\rm mrg}^{\rm MESA}$ binned as a function of merger times τ. This shows that for BBH mergers with short merger times, the factor by which COSMIC produces more BBH mergers than detailed simulations is much greater than when just considering the total as in Table 1. However, while $\mathcal{N}$ for each subpopulation is generally > 1, models using our standard $q_{\rm crit}$ criteria in COSMIC produce fewer BBH mergers with long merger times. The merger time distribution will impact the overall merger rate and the mass distribution of merging BBHs at different redshifts. Measuring the merger rate as a function of redshift can potentially help to identify how BBHs form (Fishbach & Kalogera 2021; Santoliquido et al. 2021), so it is important to have accurate predictions.

The differences in merger times shown in Figures 4 and 5 will have an impact on the resulting merger rate for BBHs. Table 2 shows the values of relative rate $\mathcal{R}_{\rm rel}$ for all model variations and donor masses. Values of this ratio close to unity result from populations where BBH mergers modeled with COSMIC and MESA occur at similar rates. Large values result from populations where COSMIC mergers are dominated by short merger times. The trends in this table follow roughly the same trends as in Table 1. However, the variation between mass subpopulations and model variations highlights how the typical merger time varies. Compared to Table 1, in some cases such as for $M_{\rm donor} = 40\ M_\odot$ with the standard model, $\mathcal{N}$ is close to unity, but this ratio $\mathcal{R}_{\rm rel}$ is much larger than unity. These results show that not only do we get more mergers from COSMIC, but the mergers are dominated by short times, which will yield a higher BBH merger rate soon after formation.

7. Conclusions

In this study we assessed how using detailed modeling of stellar physics, MT, and CE during the BH–H-rich star stage affects the final population of merging BBHs. We compared results from the rapid population synthesis code COSMIC to detailed simulations using MESA. For the models ran with MESA, we used a detailed method for MT and CE evolution (Marchant et al. 2021). We find that modeling binary evolution with detailed simulations typically results in fewer mergers and longer merger times for BBHs.

To investigate the impact of uncertainties in binary stellar evolution, we varied metallicity, allowed for super-Eddington accretion, varied the CE efficiency between $\alpha_{\rm CE} = 1$ and $\alpha_{\rm CE} = 5$, and implemented two different prescriptions for critical mass ratios for CE stability in COSMIC. For each model variation, we identified and compared regions where successful BBH mergers occurred. We calculated a number ratio $\mathcal{N}$, the ratio of the number of merging BBHs within a Hubble time between COSMIC and MESA. We also compared the distribution of merger times between the two populations and calculated a relative rate $\mathcal{R}_{\rm rel}$, the ratio of the estimated merger rate for systems modeled with COSMIC to those modeled with our detailed simulations using MESA. Our main conclusions are:

1. In all cases, models ran with COSMIC and models ran with MESA predict a different dominant formation channel for BBH mergers. Merging BBHs modeled with COSMIC are mainly formed via CE evolution. For models ran with MESA, the dominant formation channel for merging BBHs is via stable MT.
2. We find that many systems at high orbital periods, where COSMIC assumes dynamical instability and predicts successful CE ejections, actually avoid unstable MT when modeled with our MESA simulations.
3. For our models with $Z = 0.1\ Z_\odot$, we find fewer merging BBHs by up to a factor 15, and a factor of 35 for $\alpha_{\rm CE} = 5$, when using detailed stellar and binary physics with MESA compared to our models simulated with COSMIC. At solar metallicity, MESA models produce more merging BBHs than COSMIC.
4. Binaries modeled with COSMIC are dominated by much shorter merger times compared to MESA simulations. This, combined with the relative numbers results above, leads to significant differences in merger rates. COSMIC models appear to overestimate the merger rates of BBHs by factors of $\sim$ 5–500.

These results highlight how detailed modeling of stars in binary interactions can impact predictions for BBH populations and interpretation of GW sources.

Consistent with our findings, other studies assessing the stability of massive stars to MT in various contexts have also found that stars are able to maintain dynamical stability in many more configurations than are commonly assumed in rapid population synthesis codes. Moreover, other population synthesis studies that have adopted stability criteria for MT based upon stellar-structure simulations have also found a more

dominant role for stable MT in BBH formation (Neijssel et al. 2019; Bavera et al. 2021; Olejak et al. 2021; Shao & Li 2021). Our results strengthen earlier conclusions and expand the implications of the dominance of stable MT: BBH systems are formed with wider orbits and hence systematically longer merger times, and as a result, both the number of merging BBHs and the BBH merger rate can be significantly reduced.

A major current goal is to use GW observations, BBH masses, spins, and rates, in combination with binary stellar evolution predictions to assess the fraction of binaries formed through different channels (Zevin et al. 2017; Bouffanais et al. 2019; Zevin et al. 2021), and to constrain uncertain physical parameters that influence binary evolution, such as the CE efficiency (Wong et al. 2021; Bavera et al. 2021; Zevin et al. 2021), the mass-accretion efficiency (Bouffanais et al. 2021b), or the distribution metallicities across the universe (Bouffanais et al. 2021a). These constraints will become more precise as the GW source population grows (Barrett et al. 2018). However, constraints derived from models will be only as reliable and accurate as the models themselves.

Our results here, consistent with other studies, strongly motivate the need for population modeling that can account for stellar structure and evolution fully from ZAMS (not just in one particular binary phase and for a few specific mass slices, as we have done here) across the range of metallicities relevant to the formation of compact-object binaries. Parameter studies regarding initial conditions, SN kicks, and CE efficiency (despite the improved treatment used here) will still be needed, but fewer ad hoc assumptions will have to be incorporated compared to current rapid population synthesis analyses.

The authors thank Ying Qin, Aaron Dotter, Emmanouil Zapartas, and Jeff Andrews for their feedback and assistance with our MESA simulations; Scott Coughlin for assistance with computational resources; Katie Breivik and Michael Zevin for help using COSMIC; and Onno Pols and Rob Izzard for guidance of calculation of λ. We thank Tassos Fragos for insightful conversations, and thank the POSYDON collaboration for their support through the project (posydon.org). We are grateful to the referee for constructive comments on the manuscript. M.G.-G. is grateful for the support from the Ford Foundation Predoctoral Fellowship. C.P.L.B. is supported by the CIERA Board of Visitors Research Professorship. P.M. acknowledges support from the FWO junior postdoctoral fellowship No. 12ZY520N. V.K. is supported by a CIFAR G+EU Senior Fellowship, by the Gordon and Betty Moore Foundation through grant GBMF8477, and by Northwestern University. This work utilized the computing resources at CIERA provided by the Quest high performance computing facility at Northwestern University, which is jointly supported by the Office of the Provost, the Office for Research, and Northwestern University Information Technology, and used computing resources at CIERA funded by NSF PHY-1726951.

Software: Matplotlib (Hunter 2007); NumPy (van der Walt et al. 2011); Pandas (McKinney 2010).

ORCID iDs

Monica Gallegos-Garcia https://orcid.org/0000-0003-0648-2402
Christopher P L Berry https://orcid.org/0000-0003-3870-7215
Pablo Marchant https://orcid.org/0000-0002-0338-8181
Vicky Kalogera https://orcid.org/0000-0001-9236-5469

References

Abbott, B. P., Abbott, R., Abbott, T. D., et al. 2016, PhRvL, 116, 061102
Abbott, B. P., Abbott, R., Abbott, T. D., et al. 2019, PhRvX, 9, 031040
Abbott, B. P., Abbott, R., Abbott, T. D., et al. 2020, LRR, 23, 3
Abbott, R., Abbott, T. D., Abraham, S., et al. 2021a, PhRvX, 11, 021053
Abbott, R., Abbott, T. D., Abraham, S., et al. 2021b, ApJL, 915, L5
Abbott, R., Abbott, T. D., Abraham, S., et al. 2021c, SoftX, 13, 100658
Ade, P. A. R., Aghanim, N., Arnaud, M., et al. 2016, A&A, 594, A13
Agrawal, P., Hurley, J., Stevenson, S., Szécsi, D., & Flynn, C. 2020, MNRAS, 497, 4549
Antonini, F., & Rasio, F. A. 2016, ApJ, 831, 187
Antonini, F., Toonen, S., & Hamers, A. S. 2017, ApJ, 841, 77
Arca-Sedda, M., & Gualandris, A. 2018, MNRAS, 477, 4423
Asplund, M., Grevesse, N., Sauval, A. J., & Scott, P. 2009, ARA&A, 47, 481
Banerjee, S. 2021, MNRAS, 503, 3371
Barrett, J. W., Gaebel, S. M., Neijssel, C. J., et al. 2018, MNRAS, 477, 4685
Bartos, I., Kocsis, B., Haiman, Z., & Márka, S. 2017, ApJ, 835, 165
Bavera, S. S., Fragos, T., Zevin, M., et al. 2021, A&A, 647, A153
Begelman, M. C. 1979, MNRAS, 187, 237
Begelman, M. C. 2002, ApJL, 568, L97
Belczynski, K., Bulik, T., & Rudak, B. 2004, ApJL, 608, L45
Belczynski, K., Dominik, M., Bulik, T., et al. 2010, ApJL, 715, L138
Belczynski, K., Kalogera, V., & Bulik, T. 2002, ApJ, 572, 407
Belczynski, K., Kalogera, V., Rasio, F. A., et al. 2008, ApJS, 174, 223
Belczynski, K., Taam, R. E., Kalogera, V., Rasio, F. A., & Bulik, T. 2007, ApJ, 662, 504
Bondi, H., & Hoyle, F. 1944, MNRAS, 104, 273
Bouffanais, Y., Mapelli, M., Gerosa, D., et al. 2019, ApJ, 886, 25
Bouffanais, Y., Mapelli, M., Santoliquido, F., et al. 2021a, MNRAS, 507, 5224
Bouffanais, Y., Mapelli, M., Santoliquido, F., et al. 2021b, MNRAS, 505, 3873
Breivik, K., Coughlin, S., Zevin, M., et al. 2020, ApJ, 898, 71
Brott, I., de Mink, S. E., Cantiello, M., et al. 2011, A&A, 530, A115
Chaboyer, B., & Zahn, J. P. 1992, A&A, 253, 173
Charbonnel, C., & Zahn, J. P. 2007, A&A, 467, L15
Chen, H.-L., Woods, T. E., Yungelson, L. R., Gilfanov, M., & Han, Z. 2014, MNRAS, 445, 1912
Choi, J., Dotter, A., Conroy, C., et al. 2016, ApJ, 823, 102
Claeys, J. S. W., Pols, O. R., Izzard, R. G., Vink, J., & Verbunt, F. W. M. 2014, A&A, 563, A83
Claret, A., & Torres, G. 2017, ApJ, 849, 18
Cyburt, R. H., Amthor, A. M., Ferguson, R., et al. 2010, ApJS, 189, 240
de Jager, C., Nieuwenhuijzen, H., & van der Hucht, K. A. 1988, A&AS, 72, 259
de Kool, M. 1990, ApJ, 358, 189
de Mink, S. E., & Mandel, I. 2016, MNRAS, 460, 3545
Dewi, J. D. M., & Tauris, T. M. 2000, A&A, 360, 1043
Di Carlo, U. N., Giacobbo, N., Mapelli, M., et al. 2019, MNRAS, 487, 2947
Dominik, M., Belczynski, K., Fryer, C., et al. 2012, ApJ, 759, 52
du Buisson, L., Marchant, P., Podsiadlowski, P., et al. 2020, MNRAS, 499, 5941
Eggleton, P. P., Fitchett, M. J., & Tout, C. A. 1989, ApJ, 347, 998
Eldridge, J. J., & Stanway, E. R. 2009, MNRAS, 400, 1019
Eldridge, J. J., & Stanway, E. R. 2016, MNRAS, 462, 3302
Eldridge, J. J., Stanway, E. R., Xiao, L., et al. 2017, PASA, 34, e058
Ferguson, J. W., Alexander, D. R., Allard, F., et al. 2005, ApJ, 623, 585
Fishbach, M., & Kalogera, V. 2021, ApJL, 914, L30
Fragione, G., Grishin, E., Leigh, N. W. C., Perets, H. B., & Perna, R. 2019, MNRAS, 488, 47
Fragione, G., & Kocsis, B. 2018, PhRvL, 121, 161103
Fragione, G., & Kocsis, B. 2019, MNRAS, 486, 4781
Fragos, T., Andrews, J. J., Ramirez-Ruiz, E., et al. 2019, ApJL, 883, L45
Fryer, C. L., Belczynski, K., Wiktorowicz, G., et al. 2012, ApJ, 749, 91
García, F., Simaz Bunzel, A., Chaty, S., Porter, E., & Chassande-Mottin, E. 2021, A&A, 649, A114
Ge, H., Webbink, R. F., Chen, X., & Han, Z. 2015, ApJ, 812, 40
Ge, H., Webbink, R. F., & Han, Z. 2020, ApJS, 249, 9
Giacobbo, N., & Mapelli, M. 2018, MNRAS, 480, 2011
Giacobbo, N., Mapelli, M., & Spera, M. 2018, MNRAS, 474, 2959
Glebbeek, E., Gaburov, E., de Mink, S. E., Pols, O. R., & Portegies Zwart, S. F. 2009, A&A, 497, 255
Gröbner, M., Ishibashi, W., Tiwari, S., Haney, M., & Jetzer, P. 2020, A&A, 638, A119
Hamann, W. R., & Koesterke, L. 1998, A&A, 335, 1003
Han, Z., Podsiadlowski, P., & Eggleton, P. P. 1994, MNRAS, 270, 121

Heger, A., Langer, N., & Woosley, S. E. 2000, ApJ, 528, 368
Heger, A., Woosley, S. E., & Spruit, H. C. 2005, ApJ, 626, 350
Herwig, F. 2000, A&A, 360, 952
Hunter, J. D. 2007, CSE, 9, 90
Hurley, J. R., Pols, O. R., & Tout, C. A. 2000, MNRAS, 315, 543
Hurley, J. R., Tout, C. A., & Pols, O. R. 2002, MNRAS, 329, 897
Hut, P. 1981, A&A, 99, 126
Iglesias, C. A., & Rogers, F. J. 1996, ApJ, 464, 943
Inayoshi, K., Hirai, R., Kinugawa, T., & Hotokezaka, K. 2017, MNRAS, 468, 5020
Ivanova, N. 2011, ApJ, 730, 76
Izzard, R. G., Dray, L. M., Karakas, A. I., Lugaro, M., & Tout, C. A. 2006, A&A, 460, 565
Izzard, R. G., Glebbeek, E., Stancliffe, R. J., & Pols, O. R. 2009, A&A, 508, 1359
Izzard, R. G., Tout, C. A., Karakas, A. I., & Pols, O. R. 2004, MNRAS, 350, 407
Kaaz, N., Schrøder, S. L., Andrews, J. J., Antoni, A., & Ramirez-Ruiz, E. 2021, arXiv:2103.12088
King, A. R., & Begelman, M. C. 1999, ApJL, 519, L169
Kinugawa, T., Inayoshi, K., Hotokezaka, K., Nakauchi, D., & Nakamura, T. 2014, MNRAS, 442, 2963
Kippenhahn, R., Ruschenplatt, G., & Thomas, H. C. 1980, A&A, 91, 175
Klencki, J., Nelemans, G., Istrate, A. G., & Chruslinska, M. 2021, A&A, 645, A54
Klencki, J., Nelemans, G., Istrate, A. G., & Pols, O. 2020, A&A, 638, A55
Kolb, U., & Ritter, H. 1990, A&A, 236, 385
Kruckow, M. U., Tauris, T. M., Langer, N., Kramer, M., & Izzard, R. G. 2018, MNRAS, 481, 1908
Kulkarni, S. R., Hut, P., & McMillan, S. 1993, Natur, 364, 421
Kurucz, R. L. 1970, SAO Special Report 309, Smithsonian Astrophysical Observatory
Laplace, E., Justham, S., Renzo, M., et al. 2021, arXiv:2102.05036
Law-Smith, J. A. P., Everson, R. W., Ramirez-Ruiz, E., et al. 2020, arXiv:2011.06630
Mandel, I., & de Mink, S. E. 2016, MNRAS, 458, 2634
Mandel, I., & Müller, B. 2020, MNRAS, 499, 3214
Mapelli, M. 2018, arXiv:1809.09130
Marchant, P., Langer, N., Podsiadlowski, P., et al. 2017, A&A, 604, A55
Marchant, P., Langer, N., Podsiadlowski, P., Tauris, T. M., & Moriya, T. J. 2016, A&A, 588, A50
Marchant, P., Pappas, K. M. W., Gallegos-Garcia, M., et al. 2021, A&A, 650, A107
McKinney 2010, in Proc. 9th Python in Science Conf., ed. S. van der Walt & J Millman (Austin, TX: SciPy), 56
McKinney, J. C., Tchekhovskoy, A., Sadowski, A., & Narayan, R. 2014, MNRAS, 441, 3177
Mihalas, D. 1978, Stellar Atmospheres (New York: W H Freeman & Co.)
Moe, M., & Di Stefano, R. 2017, ApJS, 230, 15
Neijssel, C. J., Vigna-Gómez, A., Stevenson, S., et al. 2019, MNRAS, 490, 3740
Nelemans, G., Yungelson, L. R., Portegies Zwart, S. F., & Verbunt, F. 2001, A&A, 365, 491
Nelson, L. 2012, JPhCS, 341, 012008
Nitz, A. H., Capano, C. D., Kumar, S., et al. 2021, arXiv:2105.09151
Nitz, A. H., Dent, T., Davies, G. S., et al. 2020, ApJ, 891, 123
Nugis, T., & Lamers, H. J. G. L. M. 2000, A&A, 360, 227
Olejak, A., Belczynski, K., & Ivanova, N. 2021, A&A, 651, A100
Paczynski, B. 1976, in Structure and Evolution of Close Binary, ed. P. Eggleton, S. Mitton, & J. Whelan, Vol. 73 (Dordrecht: Reidel Publishing), 75
Patton, R. A., & Sukhbold, T. 2020, MNRAS, 499, 2803
Patton, R. A., Sukhbold, T., & Eldridge, J. J. 2021, arXiv:2106.05978
Pavlovskii, K., & Ivanova, N. 2015, MNRAS, 449, 4415
Pavlovskii, K., Ivanova, N., Belczynski, K., & Van, K. X. 2017, MNRAS, 465, 2092
Paxton, B., Bildsten, L., Dotter, A., et al. 2011, ApJS, 192, 3
Paxton, B., Cantiello, M., Arras, P., et al. 2013, ApJS, 208, 4
Paxton, B., Marchant, P., Schwab, J., et al. 2015, ApJS, 220, 15
Paxton, B., Smolec, R., Schwab, J., et al. 2019, ApJS, 243, 10
Peters, P. C., & Mathews, J. 1963, PhRv, 131, 435
Pols, O. R., Schröder, K.-P., Hurley, J. R., Tout, C. A., & Eggleton, P. P. 1998, MNRAS, 298, 525
Portegies Zwart, S. F., & McMillan, S. L. W. 2000, ApJL, 528, L17
Portegies Zwart, S. F., & Verbunt, F. 1996, A&A, 309, 179
Postnov, K. A., & Yungelson, L. R. 2014, LRR, 17, 3
Potekhin, A. Y., & Chabrier, G. 2010, CoPP, 50, 82
Puls, J., Vink, J. S., & Najarro, F. 2008, A&ARv, 16, 209
Qin, Y., Fragos, T., Meynet, G., et al. 2018, A&A, 616, A28
Rastello, S., Mapelli, M., Di Carlo, U. N., et al. 2020, MNRAS, 497, 1563
Renzo, M., Ott, C. D., Shore, S. N., & de Mink, S. E. 2017, A&A, 603, A118
Riley, J., Mandel, I., Marchant, P., et al. 2021, MNRAS, 505, 663
Ritter, H. 1988, A&A, 202, 93
Rodriguez, C. L., Kremer, K., Chatterjee, S., et al. 2021, RNAAS, 5, 19
Rodriguez, C. L., Morscher, M., Pattabiraman, B., et al. 2015, PhRvL, 115, 051101
Rogers, F. J., & Nayfonov, A. 2002, ApJ, 576, 1064
Román-Garza, J., Bavera, S. S., Fragos, T., et al. 2021, ApJL, 912, L23
Santoliquido, F., Mapelli, M., Giacobbo, N., Bouffanais, Y., & Artale, M. C. 2021, MNRAS, 502, 4877
Saumon, D., Chabrier, G., & van Horn, H. M. 1995, ApJS, 99, 713
Shao, Y., & Li, X.-D. 2021, ApJ, 920, 81
Shao, Y., Li, X.-D., & Dai, Z.-G. 2019, ApJ, 886, 118
Sigurdsson, S., & Hernquist, L. 1993, Natur, 364, 423
Spera, M., Mapelli, M., & Bressan, A. 2015, MNRAS, 451, 4086
Spera, M., Mapelli, M., Giacobbo, N., et al. 2019, MNRAS, 485, 889
Spruit, H. C. 2002, A&A, 381, 923
Stanway, E. R., & Eldridge, J. J. 2018, MNRAS, 479, 75
Stevenson, S., Vigna-Gómez, A., Mandel, I., et al. 2017, NatCo, 8, 14906
Stone, N. C., Metzger, B. D., & Haiman, Z. 2017, MNRAS, 464, 946
Thompson, T. A. 2011, ApJ, 741, 82
Timmes, F. X., & Swesty, F. D. 2000, ApJS, 126, 501
Trani, A. A., Tanikawa, A., Fujii, M. S., Leigh, N. W. C., & Kumamoto, J. 2021, MNRAS, 504, 910
Tutukov, A. V., & Yungelson, L. R. 1993, MNRAS, 260, 675
Ulrich, R. K. 1972, ApJ, 172, 165
van den Heuvel, E. P. J. 1976, in IAU Sym., Vol. 73, Structure and Evolution of Close Binary Systems, ed. P. Eggleton, S. Mitton, & J. Whelan (Cambridge: Cambridge Univ. Press), 35
van den Heuvel, E. P. J., Portegies Zwart, S. F., & de Mink, S. E. 2017, MNRAS, 471, 4256
van der Walt, S., Colbert, S. C., & Varoquaux, G. 2011, CSE, 13, 22
van Son, L. A. C., De Mink, S. E., Broekgaarden, F. S., et al. 2020, ApJ, 897, 100
Venumadhav, T., Zackay, B., Roulet, J., Dai, L., & Zaldarriaga, M. 2019, PhRvD, 100, 023011
Venumadhav, T., Zackay, B., Roulet, J., Dai, L., & Zaldarriaga, M. 2020, PhRvD, 101, 083030
Vigna-Gómez, A., MacLeod, M., Neijssel, C. J., et al. 2020, PASA, 37, e038
Vigna-Gómez, A., Toonen, S., Ramirez-Ruiz, E., et al. 2021, ApJL, 907, L19
Vink, J. S., & de Koter, A. 2005, A&A, 442, 587
Vink, J. S., de Koter, A., & Lamers, H. J. G. L. M. 2001, A&A, 369, 574
Vink, J. S., & Sander, A. A. C. 2021, MNRAS, 504, 2051
Webbink, R. F. 1984, ApJ, 277, 355
Wong, K. W. K., Breivik, K., Kremer, K., & Callister, T. 2021, PhRvD, 103, 083021
Woods, T. E., & Ivanova, N. 2011, ApJL, 739, L48
Yoon, S. C., Woosley, S. E., & Langer, N. 2010, ApJ, 725, 940
Zackay, B., Dai, L., Venumadhav, T., Roulet, J., & Zaldarriaga, M. 2019a, arXiv:1910.09528
Zackay, B., Venumadhav, T., Dai, L., Roulet, J., & Zaldarriaga, M. 2019b, PhRvD, 100, 023007
Zahn, J. P. 1977, A&A, 500, 121
Zapartas, E., Renzo, M., Fragos, T., et al. 2021, arXiv:2106.05228
Zevin, M., Bavera, S. S., Berry, C. P. L., et al. 2021, ApJ, 910, 152
Zevin, M., Pankow, C., Rodriguez, C. L., et al. 2017, ApJ, 846, 82
Zevin, M., Spera, M., Berry, C. P. L., & Kalogera, V. 2020, ApJL, 899, L1
Zhang, F., Shao, L., & Zhu, W. 2019, ApJ, 877, 87